Supplement of Biogeosciences, 13, 5719–5738, 2016
http://www.biogeosciences.net/13/5719/2016/
doi:10.5194/bg-13-5719-2016-supplement

Biogeosciences Open Access EGU

Supplement of

Examining the provenance of branched GDGTs in the Tagus River drainage basin and its outflow into the Atlantic Ocean over the Holocene to determine their usefulness for paleoclimate applications

Lisa Warden et al.

Correspondence to: Lisa Warden (lisa.warden@nioz.nl)

Supplementary Information

Sediment core descriptions

Tagus River Floodplain core (0501.029). Description has been previously published in:

Vis, G.-J., Bohncke, S. J. P., Schneider, H., Kasse, C., Coenraads-Nederveen, S., Zuurbier, K. and Rozema, J.: Holocene flooding history of the Lower Tagus Valley (Portugal), J. Quat. Sci., 25, 1222-1238, DOI: 10.1002/jqs.1401, 2010.

Mudbelt core (64PE332-30-2). Core 64PE332-30-2 retrieved from the Tagus Mudbelt consists of a fairly monotonous succession of dark olive gray homogeneous to weakly stratified sandy silt, gradually coarsening in downcore direction to silty sand. The silt and sand are composed of a mixture of siliciclastic material and bioclastic carbonate, with minute shell fragments but occasionally also intact bivalve and gastropod shells.

Lisbon Canyon Head core (64PE332-44-2). Core 64PE332-44-2 retrieved from the Lisbon Canyon head consists in its upper three meters of dark olive gray bioturbated clayey silt. Finely dispersed iron monosulphide, indicative of a strongly reduced state of the sediment, gives the sediment a dark mottled appearance. Below three meters depth the sediment turns to lighter shades of olive gray. Moving further downcore there is an increasing content of bioclastic carbonate sand. This sandy material, including foraminiferan shells and minute shell fragments, is found dispersed throughout the sediment but also locally concentrated in pockets produced by burrowing fauna. In the lower three meters towards the base of the core, the sandy material also occurs as discrete layers of a few centimeters thick, likely deposited by sediment gravity flows running down the canyon slopes. This is particularly the case for a coarse bioclastic sand layer at 778-797 cm depth, which has a sharply defined erosive lower boundary and fining upward succession typical of turbidite deposits.

Lower Setúbal Canyon core (64PE269-39). Core 64PE269-39pc was recovered from the crest of the large sediment levee bounding the lower Setúbal Canyon towards the north. In its upper half, considered in the present study and dated by AMS ^{14}C as of Holocene to Younger Dryas age, it consists of uniform olive-gray to gray bioturbated hemipelagic silty clay. From the presence of 2.5 cm of yellowish-grey oxidized sediment at the top of the core, with a thin rusty-brown iron oxide band marking the transition to reduced olive-grey sediment, it can be deduced that core recovery is fairly complete. In the lower half of the core, which on the basis of unpublished planktonic foraminiferal $\delta^{18}O$ results can be attributed to the Younger Dryas to Last Glacial Maximum, silty layers of a few millimeters thick are found intercalated in the bioturbated hemipelagic silty clay. These silty layers are interpreted to represent deposition from sediment plumes spilling over the edges of the Setúbal Canyon in the wake of major down-canyon sediment gravity flows. The silty layers are particularly abundant in the lower part of the core, where they give the sediment a distinctly laminated appearance, further accentuated by intense black iron monosulphide coloring that comes along with the silty layers. The abundance of silty layers in the lower part of the core is indicative of a prevalence of deposition from sediment gravity flows along this part of the Portuguese margin during the late glacial sea level lowstand, contrasting with hemipelagic deposition during the Holocene.

41 **Table S1:** Index abbreviations used in the text as well as a brief description, the definition of the index, end member values as well as what the

42 values indicate, and references.

Index	Brief description	Calculation	End member values	References
MBT	methylation of branched tetraethers index	MBT=(Ia+Ib+Ic)/(Ia+Ib+Ic+IIa+IIb+IIc+IIIa+IIIb+IIIc)	0.16-0.99 in global soil dataset; high value indicates a low degree of methylation	Weijers et al., 2007a
MBT'	methylation of branched tetraethers index, excluding brGDGTs that rarely occur in soils	MBT'=(Ia+Ib+Ic)/(Ia+Ib+Ic+IIa+IIb+IIc+IIIa)	0.08-1.00 in global soil dataset; high value indicates a low degree of methylation	Peterse et al., 2012
MBT'_{5ME}	methylation of branched tetraethers index excluding the 6-methyl brGDGTs	MBT'_{5Me} = (Ia+Ib+Ic)/(Ia+Ib+Ic+IIa+IIb+IIc+IIIa)	0.25-1.00 in global soil dataset; higher values indicates a low degree of methylation	De Jonge et al., 2014a
DC'	degree of cyclization, reformulated to include the pentamethylated 6-methyl brGDGTs	DC' = (Ib+IIb+IIb')/(Ia+Ib+IIa+IIb+IIa'+IIb')	0.01-0.50 in global soil dataset; high values indicative of relatively high abundances of cyclopentyl containing brGDGTs	Weijers et al., 2007a; Sinninghe Damsté et al., 2009
CBT	cyclization of branched tetraethers index	CBT=-log((Ib+IIb)/(Ia+IIa))	0-2.2 in global soil dataset; lower value indicates more cyclopentyl containing brGDGTs	Weijers et al., 2007a
CBT'	cyclization of branched tetraethers index including the 6-methyl brGDGTs	CBT' = ^{10}log[(Ic+IIa'+IIb'+IIc'+IIIa'+IIIb'+IIIc')/(Ia+IIa+IIIa)]	-2.20-0.84 in global soil dataset; higher value indicates more cyclopentyl containing brGDGTs	De Jonge et al., 2014a
BIT index	branched v. isoprenoid tetraether index; reformulated to specifiacally include the 6-methyl brGDGTs	BIT index = (Ia+IIa+IIIa+IIa'+IIIa')/(Ia+IIa+IIIa+IIa'+IIIa'+IV)	0-1; 0 indicates marine and 1 indicates terrestrial signal	Hopmans et al., 2003; De Jonge et al., 2015
IR	isomer ratio of the penta- and hexamethylated brGDGTs	IR=(IIa'+IIb'+IIc'+IIIa'+IIIb'+IIIc')/(IIa+IIb+IIc+IIIa+IIIb+IIIc+IIa'+IIb'+IIc'+IIIa'+IIIb'+IIIc')	higher value indicates more 6-methyl brGDGTs	De Jonge et al., 2015
IR_{II}	isomer ratio of non-cyclic pentamethylated brGDGTs	IR_{II}= IIa'/(IIa+IIa')	higher value indicates more pentamethylated 6-methyl brGDGTs	De Jonge et al., 2015
IR_{III}	isomer ratio of non-cyclic hexamethylated brGDGTs	IR_{III} = IIIa'/(IIIa+IIIa')	higher value indicates more hexamethylated 6-methyl brGDGTs	De Jonge et al., 2015

Table S2 Fractional abundance of brGDGTs (%).

Sample name	Relative abundance of brGDGTs (%)														
	Ia	**Ib**	**Ic**	**IIa**	**IIb**	**IIc**	**IIIa**	**IIIb**	**IIIc**	**IIa'**	**IIb'**	**IIc'**	**IIIa'**	**IIIb'**	**IIIc'**
Tagus soils															
TRS-8b	31.7	5.7	1.0	25.4	2.7	0.4	8.8	0.2	0.1	14.1	2.6	0.2	6.7	0.4	0.1
TRS-7	51.7	0.3	0.1	36.3	0.3	0.0	5.0	0.0	0.0	5.0	0.2	0.0	1.0	0.0	0.0
TRS-9	63.7	0.8	0.3	24.7	0.2	0.0	5.2	0.0	0.0	3.9	0.2	0.0	1.0	0.0	0.0
TRS-3	25.4	1.8	0.5	27.1	1.5	0.7	12.4	0.3	0.6	20.1	0.9	0.6	7.9	0.2	0.0
TRS-4	29.4	1.4	0.2	30.1	1.3	0.0	10.9	0.0	0.0	21.2	0.7	0.0	4.6	0.0	0.0
TRS-5	17.2	3.0	0.2	29.2	2.3	0.0	18.3	0.3	0.2	17.0	2.0	0.1	10.0	0.3	0.1
TRS-10	12.1	5.2	0.7	4.8	1.9	0.3	5.2	0.7	0.0	36.1	5.1	0.4	26.5	1.0	0.0
TRS-12	12.1	3.7	1.1	4.1	2.5	0.0	3.9	0.0	0.0	26.6	5.8	0.0	38.5	1.8	0.0
TRS-14b	9.1	6.2	0.9	2.9	2.9	0.2	6.0	0.6	0.2	24.2	7.6	0.5	36.4	1.9	0.3
TRS-13	8.4	2.1	0.3	7.7	1.8	0.0	12.7	0.8	0.0	30.7	3.1	0.0	31.7	0.8	0.0
TRS-15	6.8	3.1	0.4	3.1	2.0	0.1	6.9	0.2	0.1	28.3	5.1	0.1	42.7	1.0	0.0
TRS-16	7.1	1.7	0.0	1.8	1.4	0.0	3.8	0.7	0.0	23.8	4.8	0.0	53.3	1.7	0.0
TRS-20	8.5	7.4	0.0	3.3	3.6	0.0	7.7	0.0	0.0	21.4	8.9	0.0	37.2	2.0	0.0
TRS-19	8.0	6.2	2.3	3.9	4.3	1.0	3.6	0.7	0.3	21.9	16.5	0.6	27.8	2.7	0.3
Tagus Riverbank sediments															
TRS-6	21.1	9.1	3.0	14.3	4.5	0.6	10.5	0.5	0.1	12.0	6.5	1.3	15.0	1.1	0.5
TRS-8a	15.2	4.8	1.0	8.3	2.5	0.5	6.0	0.3	0.1	19.9	8.3	0.5	30.3	1.7	0.4
TRS 2a	13.4	10.8	1.4	5.8	4.4	0.2	4.4	0.4	0.1	24.0	16.3	1.1	15.1	2.3	0.3
TRS 2b	14.7	12.9	2.3	7.2	8.4	1.0	5.6	0.9	0.2	18.1	11.0	1.5	14.4	1.6	0.4
TRS 1a	19.1	6.8	0.9	11.5	1.7	0.0	9.6	0.3	0.2	24.0	5.7	0.0	18.9	1.2	0.0
TRS1b	14.2	15.8	2.9	3.8	11.1	0.2	3.1	0.4	0.1	17.2	13.2	2.3	12.6	2.6	0.6
TRS-11	11.9	4.2	1.4	6.7	2.6	0.0	9.4	0.7	1.5	24.9	6.7	0.0	27.8	2.3	0.0
TRS-14a	9.7	9.8	1.0	11.8	12.4	0.4	9.6	1.1	0.1	14.8	6.7	0.6	20.0	1.6	0.2
TRS-17	7.5	6.8	2.5	7.8	6.7	0.4	9.7	0.7	0.1	14.7	18.0	2.1	18.7	3.7	0.7
TRS-22	6.9	3.8	0.7	4.9	3.1	0.4	8.3	0.8	0.2	14.7	11.1	1.6	38.8	3.5	1.3
Tagus River SPM															
TR 2 Sup July	19.7	7.2	2.0	13.0	4.1	0.5	10.3	0.6	0.2	14.7	7.0	1.0	17.9	1.4	0.4
TR 3#1 –Sup Sept.	19.7	8.0	2.4	13.1	4.1	0.5	10.3	0.5	0.1	13.8	7.6	1.4	16.2	1.5	0.5
TR4 #1 Oct.	18.9	7.8	2.3	12.5	4.1	0.7	10.1	0.5	0.2	14.8	8.3	1.4	16.3	1.7	0.6
TR5 #1 Sup Nov.	19.4	5.7	1.2	15.3	3.7	0.5	7.5	0.5	0.1	18.7	8.0	0.7	16.3	1.7	0.4
TR 6 #1 Sup Dec.	17.2	5.7	1.4	12.5	3.7	0.4	10.9	0.5	0.1	15.8	7.0	0.8	22.1	1.6	0.4
TR7 #1 Sup Jan.	17.3	6.2	1.7	13.3	4.2	0.5	9.2	0.6	0.2	17.2	7.6	0.9	19.1	1.7	0.5
TR8 #1 Sup Feb.	19.5	7.3	2.3	13.7	4.2	0.6	10.7	0.6	0.2	14.0	6.4	1.0	17.7	1.4	0.5
TR9 #1 Sup Mar.	19.2	7.5	2.4	13.0	4.1	0.7	10.9	0.7	0.3	13.6	6.9	1.3	17.4	1.5	0.6
TR10 #1 Sup Apr.	20.1	8.1	2.6	13.4	4.4	0.6	10.2	0.6	0.2	13.4	7.1	1.5	15.8	1.4	0.6
TR11 #1 Sup May	20.8	8.3	2.8	13.3	4.3	0.6	10.9	0.5	0.2	12.5	6.6	1.3	16.1	1.4	0.5
TR12 #1 Sup June	23.0	10.0	3.7	14.2	4.9	0.7	10.1	0.7	0.4	13.3	0.0	2.2	14.2	1.7	0.9
Tagus River Floodplain sediments															
(0501.029) depth (cm)															
10	15.2	7.3	1.5	17.8	9.5	0.9	17.6	0.8	0.1	11.4	3.5	0.2	13.6	0.5	0.1

95	17.1	5.6	1.2	16.9	5.8	0.5	19.1	0.6	0.1	12.9	3.5	0.2	15.8	0.5	0.1
195	13.5	8.9	1.9	16.6	11.9	1.0	16.9	0.8	0.1	11.3	3.8	0.2	12.6	0.5	0.1
241	21.2	6.5	1.7	19.1	7.2	0.7	17.7	0.7	0.1	10.8	2.5	0.2	11.1	0.4	0.1
341.5	16.6	14.0	3.1	18.0	8.8	1.2	14.0	0.6	0.1	9.2	5.0	0.6	8.2	0.6	0.1
401	13.3	10.6	2.6	18.6	9.7	0.7	14.2	0.6	0.1	10.4	5.4	0.6	12.2	0.8	0.1
453	12.7	7.9	1.9	16.7	10.7	0.7	15.8	0.5	0.1	12.4	3.9	0.4	15.8	0.5	0.1
542	13.2	10.6	2.2	16.4	10.2	0.8	16.2	0.7	0.1	11.4	5.0	0.6	11.7	0.7	0.2
577	17.5	11.7	2.9	18.0	8.9	0.9	14.0	0.6	0.1	10.6	4.0	0.4	9.8	0.5	0.1
641	20.3	16.6	4.2	16.1	9.3	1.5	11.0	0.6	0.1	8.6	3.5	0.5	7.1	0.4	0.2
681	15.4	15.5	3.9	14.6	11.7	1.1	12.9	0.8	0.1	8.8	4.8	0.6	9.2	0.5	0.1
741	13.2	14.2	3.4	15.4	10.4	0.8	15.2	0.9	0.1	9.5	6.6	0.7	8.7	0.7	0.1
862	13.4	13.2	3.7	13.4	10.5	0.9	11.8	0.7	0.1	10.2	6.7	1.3	12.7	1.0	0.4
982	13.6	17.0	3.7	13.4	10.7	1.0	15.2	0.9	0.1	7.6	6.2	1.0	8.7	0.8	0.2
1041	15.5	16.5	3.6	14.1	10.0	0.9	13.0	0.8	0.1	9.2	5.9	0.7	8.9	0.6	0.1
Mudbelt sediments															
(64PE332-30-2) depth (cm)															
1	20.5	13.0	6.5	12.5	4.5	0.6	10.8	0.5	0.1	10.2	5.8	1.5	12.7	0.5	0.2
25	23.1	9.6	4.7	13.8	4.2	0.6	12.8	0.7	0.1	10.6	4.2	1.0	13.8	0.6	0.2
53	22.7	9.4	4.0	14.7	4.1	0.6	13.7	0.5	0.1	11.3	3.9	0.8	13.5	0.5	0.1
75	22.7	9.1	3.9	14.5	4.3	0.6	13.6	0.6	0.1	10.8	3.9	0.9	14.3	0.5	0.2
101	22.8	9.1	4.3	14.4	4.4	0.6	13.3	0.6	0.2	11.0	4.0	0.9	13.8	0.5	0.2
151	22.2	9.3	4.3	14.3	4.4	0.6	12.6	0.5	0.1	11.4	4.3	1.0	14.2	0.5	0.2
201	22.3	9.0	4.0	14.8	4.3	0.6	13.7	0.6	0.1	11.2	4.0	0.9	13.8	0.5	0.2
248	24.1	9.1	4.0	15.3	4.4	0.6	13.0	0.6	0.1	10.9	4.0	0.9	12.3	0.5	0.2
297	22.4	8.5	3.7	15.3	4.6	0.7	13.7	0.5	0.1	10.8	3.9	1.0	14.0	0.5	0.2
347	21.0	9.2	4.3	12.3	4.8	0.6	14.2	0.6	0.2	10.0	4.6	1.4	15.9	0.7	0.2
397	22.6	10.4	0.0	14.7	5.2	0.7	13.2	0.6	0.2	11.0	5.0	1.3	14.2	0.6	0.2
429	17.6	9.4	4.6	11.0	5.0	0.7	14.7	0.6	0.2	9.2	5.3	1.7	19.2	0.6	0.2
496	19.0	9.8	4.6	11.4	4.6	0.6	14.1	0.6	0.2	9.8	4.8	1.4	18.3	0.6	0.2
546	19.1	10.3	4.8	12.0	4.9	0.8	13.8	0.7	0.2	9.9	4.7	1.3	16.7	0.6	0.2
596	17.8	9.7	4.8	11.3	4.8	0.7	14.5	0.7	0.2	9.3	5.4	1.6	18.3	0.7	0.2
645	19.0	10.3	5.0	11.7	4.8	0.7	13.8	0.6	0.2	9.7	5.2	1.5	16.7	0.6	0.2
680	21.3	10.3	4.8	12.5	4.6	0.7	12.9	0.6	0.2	10.0	4.7	1.2	15.4	0.6	0.2
741	18.1	10.0	4.8	10.3	4.9	0.7	14.8	0.6	0.2	9.0	5.5	1.8	18.4	0.6	0.2
791	16.5	9.4	4.7	9.4	4.9	0.7	15.1	0.7	0.2	8.6	6.2	2.0	20.7	0.7	0.2
840	16.2	8.9	4.4	9.3	4.9	0.7	16.5	0.7	0.3	8.5	6.2	2.1	20.1	0.8	0.3
890	14.7	9.2	4.6	9.1	4.8	0.7	16.4	0.7	0.2	8.1	6.6	2.4	21.4	0.8	0.3
977	14.4	8.9	4.5	8.7	4.8	0.7	18.7	0.6	0.2	7.5	6.9	2.8	20.3	0.7	0.3
Lisbon Canyon Head sediments															
(64PE332-44-2) depth (cm)															
1	17.2	14.5	7.6	9.8	4.3	0.6	12.0	0.5	0.1	8.9	6.7	1.9	15.0	0.6	0.2
45	17.8	13.2	7.1	10.1	5.1	0.8	11.3	0.6	0.2	9.1	6.8	2.1	15.1	0.6	0.2
85	18.3	11.1	5.6	11.6	4.9	0.7	12.9	0.6	0.1	9.8	6.0	1.7	15.8	0.6	0.2
130.5	18.4	11.3	5.8	11.2	4.9	0.7	12.6	0.6	0.1	9.4	6.0	1.8	16.4	0.6	0.2
187.5	19.0	11.8	6.2	10.9	4.6	0.7	12.8	0.6	0.1	9.1	5.4	1.5	16.5	0.6	0.2
221.5	23.5	9.9	4.8	14.0	4.6	0.7	12.8	0.7	0.2	10.1	4.0	1.0	13.1	0.5	0.2

278.5	18.0	11.2	6.2	10.8	4.7	0.7	14.5	0.7	0.1	8.8	5.3	1.7	17.1	0.0	0.2
326.5	15.0	11.6	6.2	8.5	4.8	0.8	14.4	0.7	0.2	7.7	5.9	1.9	21.3	0.7	0.3
371.5	15.5	11.6	6.2	9.5	5.1	0.7	14.1	0.7	0.1	8.4	6.3	2.0	19.6	0.0	0.2
429	15.1	12.1	6.5	8.6	5.0	0.7	13.7	0.7	0.1	8.4	6.5	2.1	19.5	0.7	0.2
480	15.9	11.7	6.3	8.8	4.7	0.7	14.5	0.6	0.1	8.0	6.3	2.1	19.4	0.6	0.2
502	14.8	11.1	5.9	8.6	5.0	0.7	14.8	0.7	0.1	8.1	6.3	2.1	20.8	0.7	0.3
522	16.5	11.8	6.2	9.1	4.6	0.7	14.3	0.6	0.1	8.5	5.9	1.9	18.9	0.7	0.2
550	15.0	11.7	6.4	8.1	4.9	0.7	14.4	0.7	0.1	8.0	6.5	2.2	20.3	0.7	0.2
570	14.6	11.4	6.1	8.1	5.1	0.7	14.5	0.7	0.2	8.0	6.7	2.2	20.6	0.8	0.2
630	13.8	11.1	6.1	7.4	5.0	0.8	14.8	0.7	0.2	7.7	7.0	2.5	21.8	0.9	0.3
686	14.1	11.2	6.1	7.5	5.3	0.0	14.4	0.8	0.2	7.8	7.4	2.6	21.5	0.9	0.3
728	13.1	10.5	5.8	7.1	5.0	0.7	16.4	0.8	0.2	7.4	7.0	2.5	22.3	0.9	0.3
771	14.8	11.3	5.9	7.4	5.0	0.7	14.7	0.8	0.2	7.5	7.2	2.5	20.9	0.8	0.3
805	14.0	10.7	5.7	7.2	5.0	0.8	15.2	0.7	0.2	7.5	7.9	2.7	21.1	1.0	0.3
869.5	17.2	10.5	5.5	7.2	4.4	0.6	15.7	0.8	0.3	7.2	7.4	2.3	19.6	0.9	0.3
925.5	13.8	10.9	5.6	7.3	4.6	0.7	15.3	0.8	0.2	7.5	8.5	2.6	21.1	0.9	0.3
Lower Setúbal Canyon sediments (64PE269-39-4) depth (cm)															
1	21.7	7.8	3.9	5.7	3.0	0.5	6.6	0.6	1.6	8.5	10.7	4.4	22.3	1.6	1.1
20	15.3	6.2	3.0	5.2	1.9	0.4	8.6	0.6	0.4	7.7	9.7	3.3	33.9	2.6	1.4
40	15.8	7.0	3.5	4.8	3.0	0.5	11.0	0.4	0.2	7.4	7.9	3.1	32.7	1.8	1.1
60	12.5	7.1	3.4	4.8	2.5	0.5	10.6	0.4	0.2	7.6	11.9	4.3	30.0	2.5	1.7
80	13.5	6.3	3.3	4.2	2.7	0.5	11.2	0.5	0.2	7.2	8.0	2.9	36.6	1.9	1.0
100	15.4	6.1	3.5	4.0	2.6	0.4	12.1	0.4	0.2	7.6	7.4	3.1	35.9	1.0	0.4
120	14.4	5.6	2.7	3.7	2.0	0.3	11.1	0.4	0.5	7.2	7.7	3.0	40.2	0.7	0.4
140	12.8	5.7	3.0	3.3	3.0	0.6	13.3	0.7	0.2	6.7	6.9	3.1	37.6	2.2	1.0
160	13.3	4.5	2.0	3.6	2.4	0.4	17.5	0.8	0.2	6.3	10.7	3.9	31.2	2.0	1.2
180	14.8	4.0	3.1	5.0	3.5	0.6	14.3	0.8	0.3	7.0	12.3	4.9	26.2	2.0	1.2
200	16.3	7.7	3.7	6.6	3.3	0.7	13.4	0.7	0.2	7.2	10.2	3.9	23.9	1.5	0.8
220	13.1	5.5	4.6	5.9	3.3	0.5	15.6	0.9	0.2	6.4	14.0	5.0	22.1	1.9	1.1
240	11.8	9.7	5.0	4.6	3.8	0.5	12.0	0.8	0.2	5.8	16.0	6.3	20.2	2.0	1.4
260	15.2	8.6	4.1	4.6	3.1	0.5	12.0	0.7	0.2	6.4	13.9	5.6	21.2	2.2	1.7
280	13.2	7.6	3.8	5.0	3.1	0.6	14.0	0.8	0.2	6.5	12.0	4.8	25.6	1.6	1.2

Figure S1

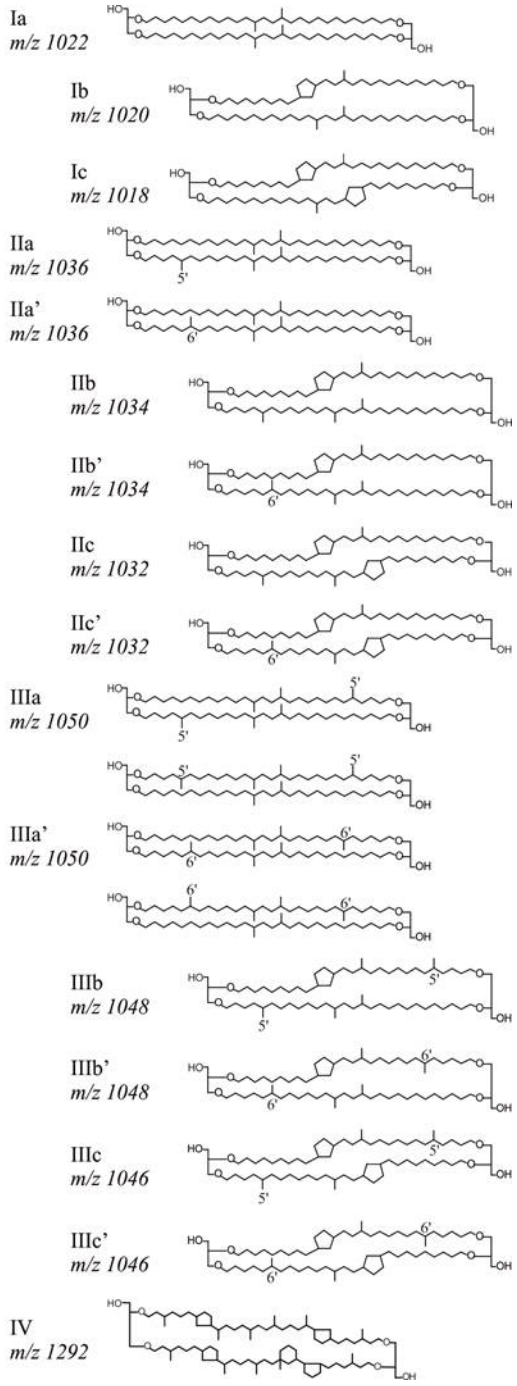

Figure S1 Chemical structures of all 15 brGDGTs (I-III) and crenarchaeol (IV) (De Jonge, et al., 2014). The compounds indicated with a prime symbol are referred to as the 6-methyl brGDGTs and the ones not designated by the prime symbol are referred to as the 5-methyl brGDGTs.

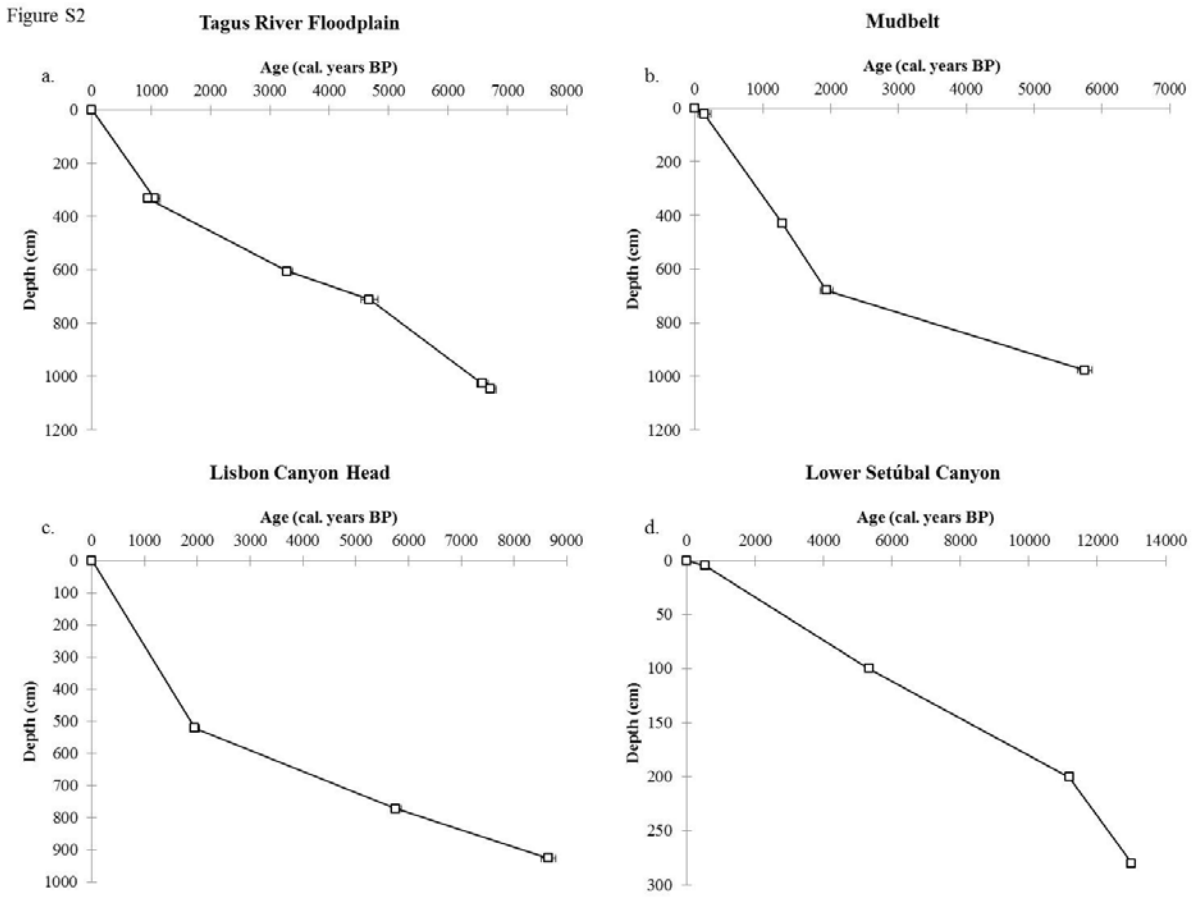

Figure S2 Depth age models for each sediment core used in this study based on the information summarized in Table 2. To create consistent chronologies for the four sediment cores, the dates were calibrated into calendar ages using the CALIB 7.0, available at http://radiocarbon.pa.qub.ac.uk/calib (Stuiver et al., 1998). The calibration data and curve selection utilized for the three marine sediment cores was Marine13 and for the Tagus River Floodplain core IntCal13 was implemented (Reimer et al., 2013). All radiocarbon dates mentioned are expressed as calibrated ages (cal. BP) and have age spans in the 2σ range.

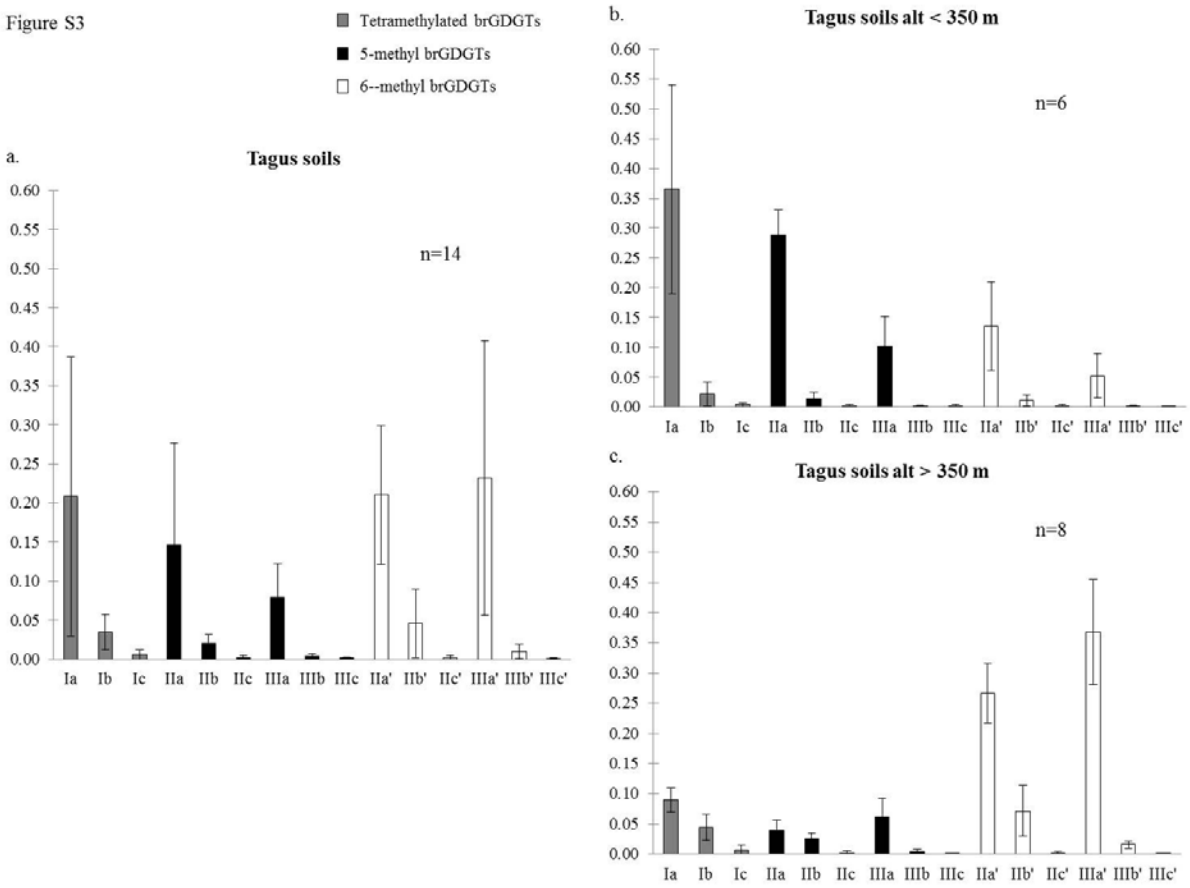

62

63 **Figure S3** Averaged brGDGT distributions in soils of the Tagus River Basin are shown in
64 panel a. Panels b-c show average brGDGT distributions for the Tagus soil samples based on
65 altitude where Tagus soils sampled below 350 m (b) are considered low altitude and Tagus
66 soils sampled above 350 m (c) are considered high altitude. Clearly the distribution of
67 brGDGTs for low altitude samples is distinct from the distribution of brGDGTs for high
68 altitude samples and the high altitude soil samples display a predominance of the 6-methyl
69 over the 5-methyl brGDGT isomers. The colors of the bars reflect the brGDGT structure as
70 labeled in the legend and the error bars represent 2xs the standard deviation.

71

72